Supplementary material for:

Socioeconomic and Atmospheric Factors Affecting Aerosol Radiative Forcing: Production-based versus Consumption-based Perspective

Jingxu Wang[a], Ruijing Ni[a], Jintai Lin[a]*, Xiaoxiao Tan[b], Dan Tong[c], Hongyan Zhao[c], Qiang Zhang[c], Zifeng Lu[d], David Streets[d], Da Pan[e], Yi Huang[f], Dabo Guan[g], Kuishuang Feng[h], Yingying Yan[a], Yongyun Hu[a], Mengyao Liu[a], Lulu Chen[a], Peng Liu[a]

Contents:

Supplementary Results:

References

---

1. Evaluation of modeled aerosol optical depth and vertical profile

Lin et al. (2016) showed that our estimated aerosol RF from global anthropogenic emissions together is close to the mean value estimated in the Intergovernmental Panel on Climate Change Fifth Assessment Report (AR5) (Boucher et al., 2013; Myhre et al., 2013). Specifically, our RF estimates are -0.48 W/m^2 for SIOA, -0.10 W/m^2 for POA and 0.32 W/m^2 for BC, consistent with the AR5 values at -0.51 W/m^2, -0.09 W/m^2 and 0.40 W/m^2, respectively. Also, Zhang et al. (2017) showed that GEOS-Chem simulated near-surface concentrations of aerosols are consistent with the satellite-inferred values used by the Global Burden of Disease 2013 study over most regions. Here we compare the simulated aerosol optical depth (AOD) to MODIS/Aqua AOD data.

Fig. S1 compares annual mean GEOS-Chem and MODIS/Aqua AOD over each of the 11 regions. MODIS data are taken from the daily level-3 collection 6 dataset (SWDB_L310, https://disc.sci.gsfc.nasa.gov/datasets/SWDB_L310_V004/summary) (Hsu et al., 2013) and mapped to the model grid (2.5⁰ long. x 2⁰ lat.), and then model results are sampled at the time and location of valid MODIS data. Following Zhang et al. (2017), we also examine locations within a region where modeled natural dusts and sea salts contribute less than 60% of AOD (red dots in Fig. 1), such that anthropogenic influence is important. Both with and without specifying the anthropogenically important locations, GEOS-Chem and MODIS/Aqua AOD are well correlated over most regions, with the correlation coefficient varying between 0.52 and 0.93 expect over Rest of World (0.24). The model bias is within 16% over five regions (East Asia, Economics in Transition, North America, South Asia, and Sub-Saharan Africa), within 24–32% over three regions (Western Europe, Middle East and North Africa, and Latin America and Caribbean), and within 40–45% over the other three regions (South-East Asia and Pacific, Pacific OECD, and Rest of World). These biases are small, considering the uncertainty in MODIS AOD data over land (0.05+20%), which could be larger regionally (Hsu et al., 2012; Sayer et al., 2012; Sayer et al., 2013). Over global land (lower right panel of Fig. 1), GEOS-Chem has a negative bias at 10% and a high correlation coefficient at 0.86 with respect to MODIS/Aqua.

Fig. S2 further shows GEOS-Chem simulated global annual average vertical distribution of mass mixing ratio (MMR) of sulfate (SO$_4$), POA and BC, for comparison to the multi-model results in Stjern et al. (2016). The MMR of sulfate ranges from 0.7 µg/kg at surface to about 0.1 µg/kg near the tropopause. For POA, the MMR is below 0.7 µg/kg at all height. The distributions are comparable to the GEOS-Chem Ajoint model results in Stjern et al. (2016). The MMR of BC here (0–0.07 µg/kg) is slightly lower than the GEOS-Chem Ajoint results in Stjern et al. (2016), because of strengthened wet scavenging of BC (Wang et al., 2014) implemented here but not in their model. The range of MMR at surface is large among the 10 models in Stjern et al. (2016): about 0.4–1.4 µg/kg for sulfate, 0.6–3.7 µg/kg for POA, and 0.10–0.22 µg/kg for BC. Compared to the inter-model median of MMR in Stjern et al. (2016), our result is comparable for sulfate and about 30% lower for POA and BC. These comparison results suggest that our aerosol simulation is reasonable for subsequent analysis of RF
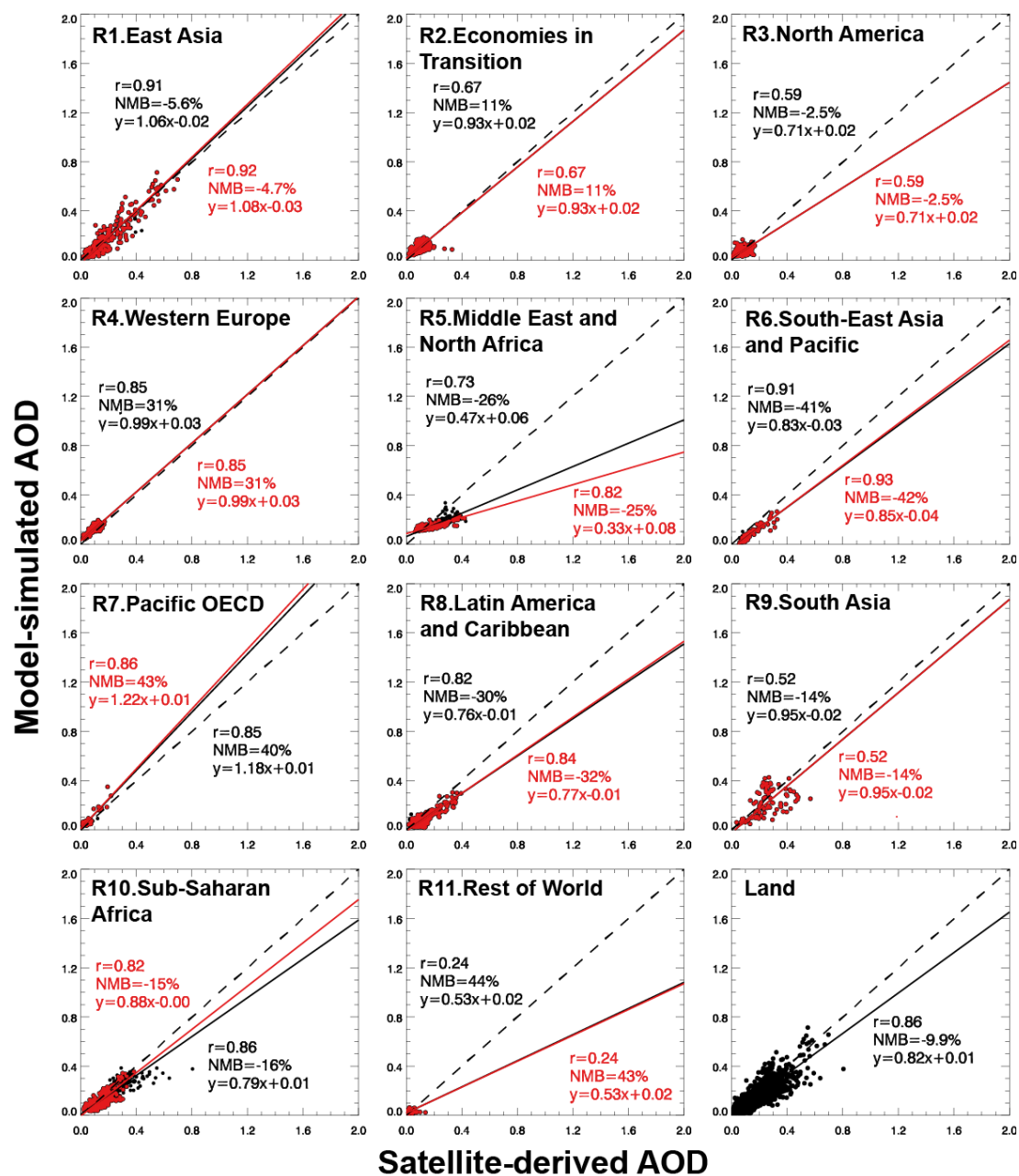
drivers.

Fig. S1. Scatterplot and statistical analysis for GEOS-Chem AOD relative to MODIS/Aqua AOD over 11 regions and over global land. In any panel, each dot represents annual mean AOD at a location (i.e., a 2.5^0 long. x 2^0 lat. grid cell). The locations with modeled natural dusts and sea salts together contributing less than 60% of total AOD are marked red.
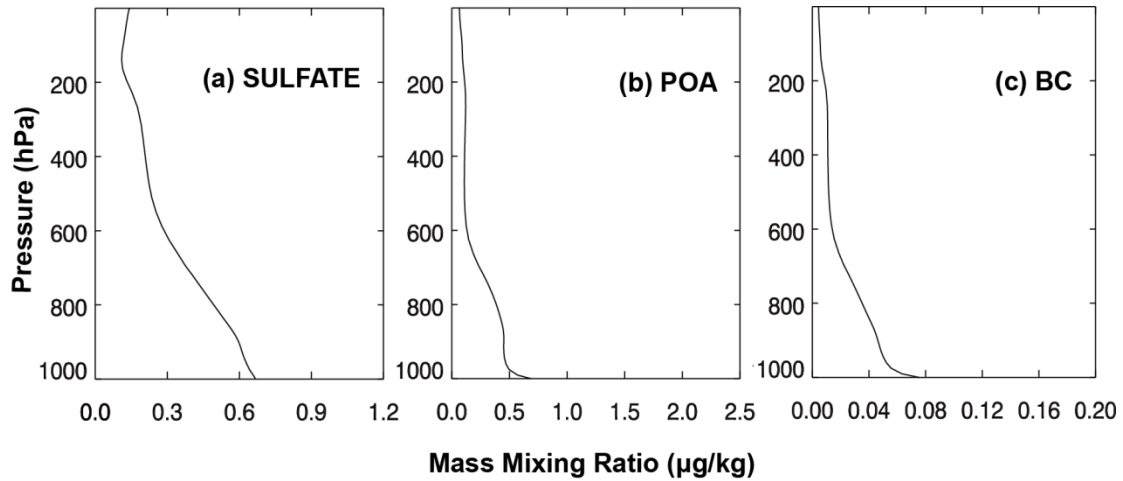
Fig. S2. Global annual average vertical profiles of mass mixing ratios (MMR) of (a) sulfate, (b) POA and (c) BC.

2. Comparison of CE_p and per emission RF_p to previous studies

Table S1 compares our calculated CE_p to Stjern et al. (2016) and Reddy and Boucher (2007). For sulfate and POA, our results are generally comparable to Stjern et al. (2016), although there is a notable difference for Western European sulfate and for POA of Middle East and North Africa. For BC, our results are within 0.2–2.5 days of Stjern et al. (2016) and Reddy and Boucher (2007). These differences are small compared to the cross-model spread shown in Stjern et al. (2016).

Table S2 further presents RF_p per unit of E_p (i.e., the product of CE_p and RE_p), for additional comparison with multi-model mean results for the year 2000 in HTAP (2010). Results are available from both studies for East Asia, North America and South Asia, although we define a region as its territory while HTAP defines a region as a large rectangular area encompassing that region. For POA, our values are generally higher than the mean values in HTAP by a factor of 1.3–2.5 (region dependent). For BC, our results are close to HTAP, except that our value for South Asia (65.0 mW/m^2/Tg·yr) is slightly above the mean plus one standard deviation in HTAP.

Table S1: Comparison of production-based chemical efficiency (CE$_p$).

	CE of Sulfate (day)		CE of POA (day)		CE of BC (day)		
	Our work	Stjern et al. [1]	Our work	Stjern et al. [1]	Our work	Stjern et al. [1]	Reddy et al. [2]
East Asia	3.0	2.9 (2.8–4.9)	5.4	4.9 (1.9–10.2)	5.4	5.6 (4.5–9.2)	4.6
Economies in Transition	2.8		5.2	4.1 (2.5–10.1)	5.4	4.5 (4.5–8.8)	
North America	1.7	1.6 (1.6–5.9)	4.1	4.0 (0.2–17.5)	4.2	5.1 (4.0–10.5)	4.8
Western Europe	2.3	3.3 (3.1–7.1)	4.1	4.9 (0.9–14.6)	4.3	5.5 (5.5–12.2)	5.0
Middle East and North Africa	5.8		7.7	10.1 (10.1–24.5)	8.5	10.5 (1.4–11.7)	7.3
Pacific OECD	2.0		3.4		3.4		4.6
Latin America and Caribbean	2.5		4.7		4.4		5.3
South Asia	2.7	2.4 (2.4–10.5)	7.1	6.6 (2.1–21.9)	5.9	8.4 (6.6–14.1)	6.6
Sub-Saharan Africa	4.3		6.2		5.7		7.2

1. The model results are based on GEOS-Chem Adjoint for 2010. The range of model results across the 10 models are also shown in parentheses.

2. The model results are based on LMD GCM for 2000.

Table S2: Comparison of RF$_p$ per unit of E$_p$.

	POA (mW/m^2/Tg)		BC (mW/m^2/Tg)	
	Our work	HTAP	Our work	HTAP
East Asia	-6.3	-3.4±1.1	52.1	43.4±23.0
North America	-5.5	-4.4±1.2	42.2	42.0±14.7
South Asia	-9.2	-3.7±1.0	65.0	37.6±17.5

References

Boucher, O., Randall, D., Artaxo, P., Bretherton, C., Feingold, G., Forster, P., Kerminen, V.-M., Kondo, Y., Liao, H., Lohmann, U., 2013. Clouds and aerosols, Climate change 2013: the physical science basis. Contribution of Working Group I to the Fifth Assessment Report of the Intergovernmental Panel on Climate Change. Cambridge University Press, pp. 571-657.

Hsu, N., Gautam, R., Sayer, A., Bettenhausen, C., Li, C., Jeong, M., Tsay, S.-C., Holben, B., 2012. Global and regional trends of aerosol optical depth over land and ocean using SeaWiFS measurements from 1997 to 2010. Atmospheric Chemistry and Physics 12, 8037.

Hsu, N.C., Sayer, A.M., Jeong, M.-J., Bettenhausen, C., 2013. SeaWiFS Deep Blue Aerosol Optical Depth and Angstrom Exponent Daily Level 3 Data Gridded at 1.0 Degrees V004. Goddard Earth Sciences Data and Information Services Center (GES DISC).

HTAP, 2010. Hemispheric Transport of Air Pollution, Part A: Ozone and particulate matter, Geneva, Switzerlang.

Lin, J., Tong, D., Davis, S.J., Ni, R., Tan, X., Pan, D., Zhao, H., Lu, Z., Streets, D.G., Feng, T., 2016. Global climate forcing of aerosols embodied in international trade. Nature Geoscience 9, 790-794.

Myhre, G., Shindell, D., Bréon, F.-M., Collins, W., Fuglestvedt, J., Huang, J., Koch, D., Lamarque, J.-F., Lee, D., Mendoza, B., 2013. Anthropogenic and natural radiative forcing. Climate change 423.

Reddy, M.S., Boucher, O., 2007. Climate impact of black carbon emitted from energy consumption in the world's regions. Geophysical Research Letters 34.

Sayer, A., Hsu, N., Bettenhausen, C., Jeong, M., Holben, B., Zhang, J., 2012. Global and regional evaluation of over-land spectral aerosol optical depth retrievals from SeaWiFS.

Sayer, A., Hsu, N., Bettenhausen, C., Jeong, M.J., 2013. Validation and uncertainty estimates for MODIS Collection 6 "Deep Blue" aerosol data. Journal of Geophysical Research: Atmospheres 118, 7864-7872.

Stjern, C.W., Samset, B.H., Myhre, G., Bian, H., Chin, M., Davila, Y., Dentener, F., Emmons, L.K., Flemming, J., Haslerud, A.S., 2016. Global and regional radiative forcing from 20 % reductions in BC, OC andSO 4 – an HTAP2 multi-model study. Atmospheric Chemistry and Physics 16, 13579-13599.

Wang, Q., Jacob, D.J., Spackman, J.R., Perring, A.E., Schwarz, J.P., Moteki, N., Marais, E.A., Ge, C., Wang, J., Barrett, S.R., 2014. Global budget and radiative forcing of black carbon aerosol: Constraints from pole-to-pole (HIPPO) observations across the Pacific. Journal of Geophysical Research: Atmospheres 119, 195-206.

Zhang, Q., Jiang, X., Tong, D., Davis, S.J., Zhao, H., Geng, G., Feng, T., Zheng, B., Lu, Z., Streets, D.G., Ni, R., Brauer, M., van Donkelaar, A., Martin, R.V., Huo, H., Liu, Z., Pan, D., Kan, H., Yan, Y., Lin, J., He, K., Guan, D., 2017. Transboundary health impacts of transported global air pollution and international trade. Nature 543, 705-709.